Progress In Electromagnetics Research, Vol. 134, 189–208, 2013

DEVELOPMENT OF A NEW APPROACH FOR HIGH-QUALITY QUADRUPLING FREQUENCY OPTICAL MILLIMETER-WAVE SIGNAL GENERATION WITHOUT OPTICAL FILTER

Nael A. Al-Shareefi[1, *], Syed I. S. Hassan[2], Fareq Malek[2], Razali Ngah[3], Syed A. Aljunid[1], Rashid A. Fayadh[1], Jaafar A. ALdhaibani[1], and Hasliza A. Rahim[1]

[1]School of Computer and Communication Engineering, Universiti Malaysia Perlis (UniMAP), Taman, Seberang Jaya Fasa 3, Kuala Perlis, Perlis 02000, Malaysia

[2]School of Electrical System Engineering, Universiti Malaysia Perlis (UniMAP), Pauh Putra, Arau, Perlis 02600, Malaysia

[3]Faculty of Electrical Engineering, Universiti Teknologi Malaysia, Malaysia

Abstract—In this paper, we propose a new approach to generate quadrupling-frequency optical millimeter-wave (mm-wave) signal with carrier suppression by using two parallel Mach-Zehnder modulators (MZMs) in Radio-over-fiber (RoF) system. Among the numerous properties of this approach, the most important is that a filterless optical mm-wave at 60 GHz with an optical sideband suppression ratio (OSSR) as high as 40 dB can be obtained when the extinction ratio of the MZM is 25 dB. Simplicity and cost-effectiveness have made this approach a compelling candidate for future wave-division-multiplexing RoF systems. Theoretical analysis is conducted to suppress the undesired optical sidebands for the high-quality generation of frequency quadrupling mm-wave signal. The simulation results show that a 60 GHz mm-wave is generated from a 15 GHz radio frequency (RF) oscillator with an OSSR as high as 40 dB and an radio frequency spurious suppression ratio (RFSSR) exceeding 35 dB without any optical or electrical filter when the extinction ratio of the MZM is 25 dB. Furthermore, the effect of the non-ideal RF-driven voltage as well as the phase difference of RF-driven signals applied to the two MZMs on OSSR and RFSSR is discussed and analyzed. Finally, we

Received 4 October 2012, Accepted 9 November 2012, Scheduled 24 November 2012

* Corresponding author: Nael Ahmed Al-Shareefi (naelahmed2000@yahoo.com).

establish a RoF system through simulation to verify the transmission performance of the proposed scheme. The Q-factor performance and eye patterns are given.

1. INTRODUCTION

Radio-over-fiber (RoF) is a type of communication technology that combines millimeter-wave (mm-wave) with optical communication [1–7]. RoF has attracted considerable attention for its potential application in future broadband wireless access networks because of its advantages of extremely low propagation loss, unlimited fiber bandwidth, immunity to electromagnetic interference, and high spatial division multiplexing on account of large atmospheric attenuation [8–11]. In an RoF system, the cost-effective and high quality generation of high frequency mm-wave signals is a key technology that requires further development toward high-frequency bands, especially for frequencies above 40 GHz [12–14]. Compared with the conventional electrical method, the optical method is preferable [15–17]. By beating the two high-order optical sidebands with good coherence in a square-law photodetector (PD), a laser with an optical external phase or intensity modulator is a promising and attractive technology for the generation of high-frequency mm-wave signals, the frequency of which can be several-folds that of the radio frequency (RF) local oscillator [18–33]. In this technology, a high optical sideband suppression ratio (OSSR) is extremely desirable for the generation of high-quality mm-wave signals.

Several different approaches have been recently proposed to generate frequency quadrupling mm-wave signal. By employing two cascaded Mach-Zehnder modulators (MZMs), Zhao conducted both a theoretical investigation and an experimental verification for the generation of frequency quadrupling mm-wave signal [34]. However, the undesired optical sidebands were not well suppressed. Thus, only a lower OSSR of 25 dB can be obtained, which degrades the RF spurious suppression ratio (RFSSR) between the desired frequency quadrupling mm-wave signal and other undesired RF components. Based on an integrated Mach-Zehnder modulator, which consists of three sub-MZMs, namely, MZM-a, MZM-b, and MZM-c, Lin demonstrated a novel frequency quadrupling technique for generating optical mm-waves [12]. In this technique, two sub-MZMs (MZM-a and MZM-b) are biased at the maximum transmission point with 90° phase shift between the driving signals. MZM-c is biased at the minimum transmission point. However, in order to achieve high OSSR, a modulation index of π is needed for driving the integrated MZM. This

suggests that a high RF power is required, i.e., not cost effective. Liu also proposed a scheme to generate frequency quadrupling mm-wave signal based on a 1×4 Multimode interference (MMI) coupler with four optical phase-modulator arms [35]. However, the relative optical phase introduced by the MMI coupler is difficult to control [36].

In this paper, we propose a new frequency quadrupling approach that can generate a carrier-suppressed optical mm-wave signal by using two commercially available dual-electrode MZMs (DE-MZMs). Both MZMs are biased at the minimum transmission point. The dual electrodes of the two MZMs are driven by the same RF sinusoid with 90° phase shift. Two optical sidebands of second-order optical harmonics related to the optical carrier are generated and maximized at the output of the modulator, and the two sidebands have a frequency spacing of four times of the driving RF to the MZMs. With a modulation index of 2.404, a cost-effective optical mm-wave at 60 GHz with an OSSR as high as 40 dB and an RFSSR exceeding 35 dB is obtained without any optical or electrical filter when the extinction ratio of the MZM is 25 dB. Given that the optical carrier and undesired optical sidebands are well suppressed, the high-quality optical mm-wave signal does not suffer from power fading induced by fiber dispersion. The effects of non-ideal RF-driven voltage and phase difference between RF-driven signals applied to the two MZMs on OSSR and RFSSR are studied through simulation. Finally, in terms of the Q-factor and eye pattern of the system, the performance of the generated optical mm-wave after transmission over fiber is also investigated.

The remainder of paper is organized as follows: In Section 2, theoretical model of frequency quadrupling technique is built by using the proposed approach. Section 3 details the simulation results and discussion. Finally, the conclusion is given in Section 4.

2. OPERATION PRINCIPLE

The schematic diagram for frequency quadrupling mm-wave signal generation is proposed as shown in Fig. 1. A continuous lightwave emitted from the LD expressed as $E_0 \exp(jw_0t)$, where E_0 is the amplitude of the optical field, and $w_0 = 2\pi f_0$ is the angular frequency of the optical carrier, is split into two branches, namely, I and II, by a 3-dB optical splitter. Each branch has a DE-MZM, that is, MZM-a in branch I and MZM-b in branch II. A 180° phase shift is introduced between the RF-driven signals applied to MZM-a and MZM-b. The RF-driven signals are applied to the four arms of the two MZMs with different phase shifts introduced by electrical phase

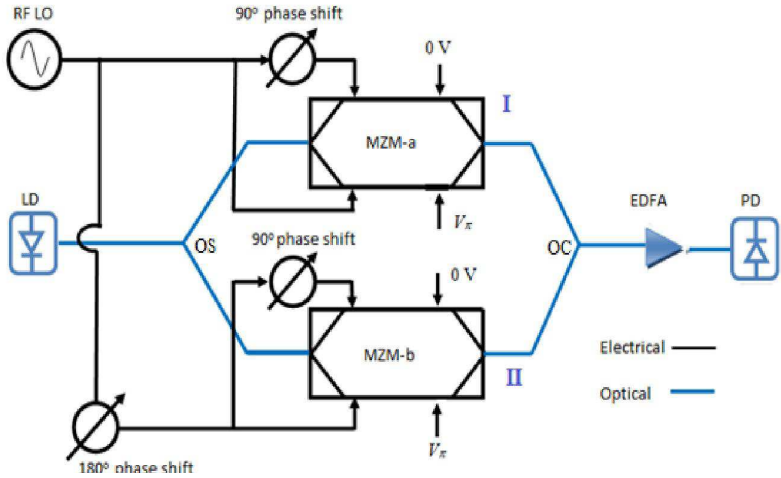

Figure 1. The proposed quadrupling-frequency mm-wave generation scheme with two parallel MZMs. (LD: laser diode; MZM: dual-electrode Mach-Zehnder modulator; RF LO: radio frequency local oscillator; OS: optical splitter; OC: optical coupler; PD: photo diode;EDFA: erbium-doped fiber amplifier).

shifters, and the four arms are biased by different DC voltages, as depicted in Fig. 1. Thus, the RF-driven signals applied to the four arms are $V_{RF}\cos(w_{RF}t+\pi/2)$, $V_{RF}\cos(w_{RF}t)$, $V_{RF}\cos(w_{RF}t+\pi/2)$, and $V_{RF}\cos(w_{RF}t)$, where V_{RF} and w_{RF} are the amplitude and angular frequency of the RF-driven signal, respectively. If the insertion loss attenuation of the MZM is neglected, and the extinction ratio is assumed to be infinite, the optical field at the output of the optical coupler (OC) can be written as

$$E_{out}(0,t) = E_I(0,t) + E_{II}(0,t) \tag{1}$$

$$\begin{aligned} E_I(0,t) &= \frac{E_0}{4}e^{jw_0t}\left[e^{j\frac{\pi}{V_\pi}V_{RF}\cos(w_{RF}t+\frac{\pi}{2})} + e^{j\frac{\pi}{V_\pi}V_{RF}\cos(w_{RF}t)}\cdot e^{j\frac{V_{dc}}{V_\pi}\cdot\pi}\right] \\ &= \frac{E_0}{4}e^{jw_0t}\left[e^{j\frac{\pi}{V_\pi}V_{RF}\cos(w_{RF}t+\frac{\pi}{2})} + e^{j\frac{\pi}{V_\pi}V_{RF}\cos(w_{RF}t)}\cdot e^{j\pi}\right] \\ &= \frac{E_0}{4}e^{jw_0t}\left[e^{jm\cos(w_{RF}t+\frac{\pi}{2})} - e^{jm\cos(w_{RF}t)}\right] \end{aligned} \tag{2}$$

By applying the Jaccobi-Anger expansion

$$e^{jx\sin(\Omega t)} = \sum_{n=-\infty}^{\infty} J_n(x)e^{jn\Omega t}, \quad e^{jx\cos(\Omega t)} = \sum_{n=-\infty}^{\infty} j^n J_n(x)e^{jn\Omega t} \tag{3}$$

to Eq. (2), $E_I(0,t)$ becomes

$$\begin{aligned}
&E_I(0,t)\\
&= \frac{E_0}{4}\, e^{jw_0t}\left[\sum_{n=-\infty}^{\infty} j^n J_n(m) e^{jn\left(w_{RF}t+\frac{\pi}{2}\right)} - \sum_{n=-\infty}^{\infty} j^n J_n(m) e^{jn(w_{RF}t)}\right]\\
&= \frac{E_0}{4}\, e^{jw_0t}\left[\sum_{n=-\infty}^{\infty} J_n(m) e^{j(nw_{RF}t+n\pi)} - \sum_{n=-\infty}^{\infty} J_n(m) e^{j\left(nw_{RF}t+\frac{n\pi}{2}\right)}\right]\\
&= \frac{E_0}{4}\, e^{jw_0t}\left[\sum_{n=-\infty}^{\infty} J_n(m) e^{j\left(nw_{RF}t+\frac{3n\pi}{4}+\frac{n\pi}{4}\right)}\right.\\
&\quad \left. - \sum_{n=-\infty}^{\infty} J_n(m) e^{j\left(nw_{RF}t+\frac{3n\pi}{4}-\frac{n\pi}{4}\right)}\right]\\
&= \frac{E_0}{4}\, e^{jw_0t}\left[\sum_{n=-\infty}^{\infty} J_n(m)\cdot e^{j(nw_{RF}t+\frac{3n\pi}{4})}\left\{e^{j(\frac{n\pi}{4})} - e^{-j(\frac{n\pi}{4})}\right\}\right]\\
&= \frac{E_0}{2} \sum_{n=-\infty}^{\infty} J_n(m)\, \sin\left(\frac{n\pi}{4}\right) e^{j\left[(w_0+nw_{RF})t+\frac{3n\pi}{4}\right]} \qquad (4)
\end{aligned}$$

where V_π is the switching voltage of MZM, m the RF modulation index defined as $m = (\frac{V_{RF}}{v_\pi}, \pi)$, and J_n the nth order Bessel function

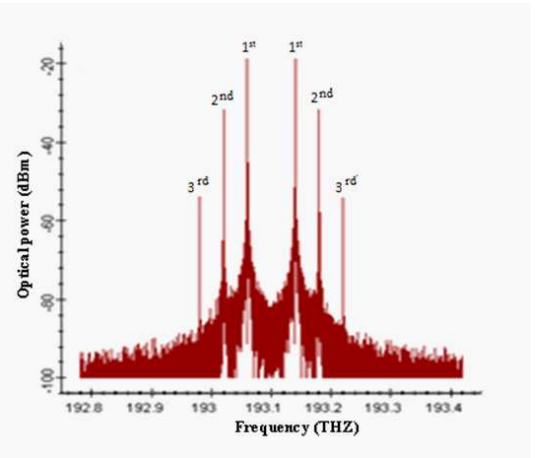

Figure 2. Simulated optical spectra of the generated optical mm-wave with the DE-MZM biased at the minimum transmission point with 90° phase shift introduced between the RF-driving signals applied to each drive electrode.

of the first kind. Equation (4) shows that the $(4n)$ th-order optical sidebands are suppressed because of the term $\sin(\frac{n\pi}{4})$, as shown in Fig. 2. Similarly, the optical mm-wave exported from MZM-b can be described as

$$E_{II}(0,t) = \frac{E_0}{2} \sum_{n=-\infty}^{\infty} J_n(m) \sin\left(\frac{n\pi}{4}\right) e^{j\left[(w_0+nw_{RF})t-\frac{n\pi}{4}\right]} \tag{5}$$

Thus, the optical field at the output of the OC can be expressed as

$$\begin{aligned}
& E_{out}(0,t) \\
= \; & \frac{E_0}{2}\left[\sum_{n=-\infty}^{\infty} J_n(m)\sin\left(\frac{n\pi}{4}\right)e^{j\left[(w_0+nw_{RF})t+\frac{3n\pi}{4}\right]}\right. \\
& \left. + \sum_{n=-\infty}^{\infty} J_n(m)\sin\left(\frac{n\pi}{4}\right)e^{j[(w_0+nw_{RF})t-\frac{n\pi}{4}]}\right] \\
= \; & \frac{E_0}{2}\left[\sum_{n=-\infty}^{\infty} J_n(m)\sin(\frac{n\pi}{4})e^{j[(w_0+nw_{RF})t+\frac{n\pi}{2}+\frac{n\pi}{4}]}\right. \\
& \left. + \sum_{n=-\infty}^{\infty} J_n(m)\sin\left(\frac{n\pi}{4}\right)e^{j\left[(w_0+nw_{RF})t-\frac{n\pi}{2}+\frac{n\pi}{4}\right]}\right] \\
= \; & E_0 e^{jw_0t}\left[\sum_{n=-\infty}^{\infty} J_n(m)e^{j((w_0+nw_{RF})t+\frac{n\pi}{4})}\left\{e^{j(\frac{n\pi}{2})}-e^{-j(\frac{n\pi}{2})}\right\}\right] \\
= \; & E_0 \sum_{n=-\infty}^{\infty} J_n(m)\sin\left(\frac{n\pi}{4}\right)\cos\left(\frac{n\pi}{2}\right)\exp\left[j(w_0+nw_{RF})t+\frac{n\pi}{4}\right]
\end{aligned} \tag{6}$$

Equation (6) shows that the nth-order sidebands are all suppressed, except for $n = 4k-2$, where k is an integer. Eq. (6) also shows that the $(4k-2)$ th-order sidebands interfere constructively and that the odd-order sidebands destructively interfere at the output coupler. This is because the 180° phase shift between the RF-driven signals applied to the two MZMs causes the polarities of the odd-order sidebands at the output of MZM-a to oppose those at the output of MZM-b. Therefore, after the output coupler, only the optical sidebands of the order of second, sixth, and tenth remain, as depicted in Fig. 3(a).

Within the typical modulation index range of $0 \leq m \leq 2.4048$, the Bessel function J_{4k-2} monotonically reduces with m. At $m = 2.4048$, the corresponding values of $J_2(m)$, $J_6(m)$ and $J_{10}(m)$ are 0.4318, 0.0034, and 1.5252×10^{-6}, respectively, as shown in Fig. 4. Therefore, the optical sidebands higher than the sixth order can be neglected

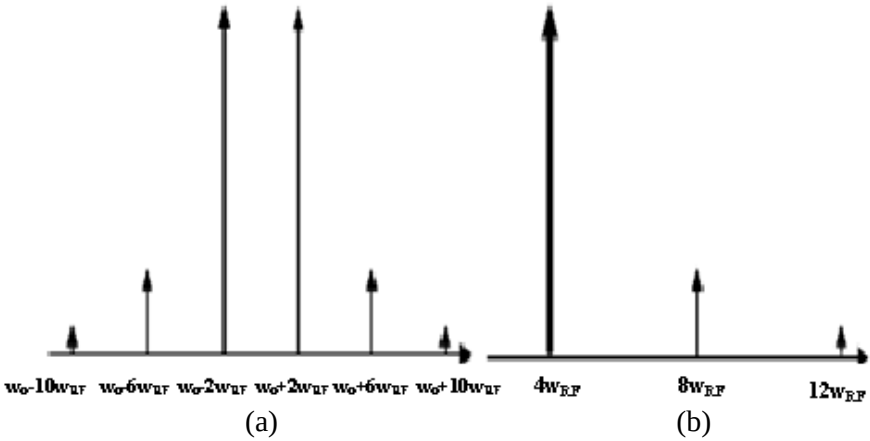

Figure 3. (a) Optical, (b) electrical spectrum of the mm-wave signals.

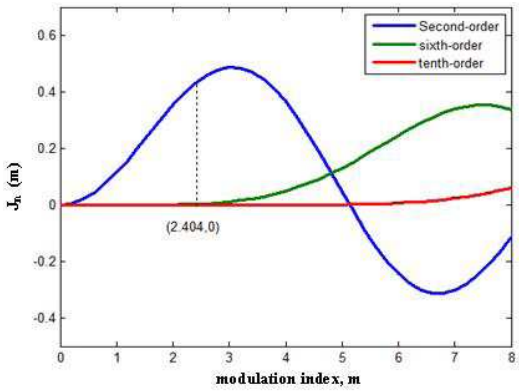

Figure 4. Bessel Function of first kind.

because of their extremely low power. Thus, Eq. (6) can be simplified as

$$E_{out}(0,t) = E_0\Big\{J_2(2.4048)\left[e^{j[(w_0-2w_{RF})t-\frac{\pi}{2}]} - e^{j[(w_0+2w_{RF})t+\frac{\pi}{2}]}\right] + J_6(2.4048)\left[e^{j[(w_0+6w_{RF})t+\frac{3\pi}{2}]} - e^{j[(w_0-6w_{RF})t-\frac{3\pi}{2}]}\right]\Big\} \quad (7)$$

By using Eq. (7), the OSSR for the MZM with infinite extinction ratio is given by

$$\text{OSSR} = 10\log\left[\frac{J_2(2.4048)^2}{J_6(2.4048)^2}\right] = 42.07\,\text{dB} \quad (8)$$

In a back-to-back (B-T-B) case, the quadrupling-frequency the optical mm-wave signal is detected by using a square-law PD, and its photocurrent can be written as

$$\begin{aligned} I(0,t) &= \Re\,|E_{out}(0,t)|^2 = \Re E_0^2 \cdot [E_{out}(0,t) \cdot E_{out}(0,t)^*] \\ &= \Re E_0^2 \Big[J_2(m)\, e^{j[(w_0-2w_{RF})t]} e^{-j\frac{\pi}{2}} - J_2(m) e^{j[(w_0+2w_{RF})t]} e^{j\frac{\pi}{2}} \\ &\quad + J_6(\mathrm{m}) e^{j[(w_0+6w_{RF})t]} e^{j\frac{3\pi}{2}} - J_6(\mathrm{m}) e^{j[(w_0-6w_{RF})t]} e^{-j\frac{3\pi}{2}} \Big] \\ &\quad \cdot \Big[J_2(m)\, e^{-j[(w_0-2w_{RF})t]} e^{j\frac{\pi}{2}} - J_2(m)\, e^{-j[(w_0+2w_{RF})t]} e^{-j\frac{\pi}{2}} \\ &\quad + J_6(\mathrm{m}) e^{-j[(w_0+6w_{RF})t]} e^{-j\frac{3\pi}{2}} - J_6(\mathrm{m}) e^{-j[(w_0-6w_{RF})t]} e^{j\frac{3\pi}{2}} \Big] \quad (9) \end{aligned}$$

where $\Re$ is the photodiode responsivity, and $E_{out}(0,t)^*$ stands for the complex conjugate of $E_{out}(0,t)$. Equation (9) can be further simplified to

$$\begin{aligned} I(0,t) &= \Re E_0^2 \Big[J_2^2 - J_2^2 e^{j[(w_0-2w_{RF}-w_0-2w_{RF})t]} e^{-j\pi} \\ &+ J_2 J_6 e^{j[(w_0-2w_{RF}-w_0-6w_{RF})t]} e^{-j2\pi} \\ &- J_2 J_6 e^{j[(w_0-2w_{RF}-w_0+6w_{RF})t]} e^{j\pi} + J_2^2 - J_2^2 e^{j[(w_0+2w_{RF}-w_0+2w_{RF})t]} e^{j\pi} \\ &- J_2 J_6 e^{j[(w_0+2w_{RF}-w_0-6w_{RF})t]} e^{-j\pi} + J_2 J_6 e^{j[(w_0+2w_{RF}-w_0+6w_{RF})t]} e^{j2\pi} \\ &+ J_6^2 - J_6^2 e^{j[(w_0+6w_{RF}-w_0+6w_{RF})t]} e^{j3\pi} + J_2 J_6 e^{j[(w_0+6w_{RF}-w_0+2w_{RF})t]} e^{j2\pi} \\ &- J_2 J_6 e^{j[(w_0+6w_{RF}-w_0-2w_{RF})t]} e^{j\pi} + J_6^2 - J_6^2 e^{j[(w_0-6w_{RF}-w_0-6w_{RF})t]} e^{-j3\pi} \\ &+ J_2 J_6 e^{j[(w_0-6w_{RF}-w_0-2w_{RF})t]} e^{-j2\pi} - J_2 J_6 e^{j[(w_0-6w_{RF}-w_0+2w_{RF})t]} e^{-j\pi} \Big] \\ &= \Re E_0^2 \big[J_2^2 + J_2^2 e^{-j4w_{RF}t} + J_2 J_6 e^{-j8w_{RF}t} - J_2 J_6 e^{j4w_{RF}t} \\ &+ J_2^2 + J_2^2 e^{j4w_{RF}t} + J_2 J_6 e^{-j4w_{RF}t} + J_2 J_6 e^{j8w_{RF}t} \\ &+ J_6^2 + J_6^2 e^{j12w_{RF}t} + J_2 J_6 e^{j4w_{RF}t} + J_2 J_6 e^{j8w_{RF}t} \\ &+ J_6^2 + J_6^2 e^{-j12w_{RF}t} + J_2 J_6 e^{-j4w_{RF}t} + J_2 J_6 e^{-j8w_{RF}t} \big] \\ &= \Re E_0^2 \big[2J_2^2 + 2J_6^2 + 2J_2^2 \cos 4w_{RF}t \\ &+ 2J_2 J_6 \cos 4w_{RF}t + 2J_2 J_6 \cos 4w_{RF}t \\ &+ 2J_2 J_6 \cos 8w_{RF}t + 2J_2 J_6 \cos 8w_{RF}t + 2J_6^2 \cos 12w_{RF}t \big] \\ &= \Re E_0^2 \big[2J_2^2 + 2J_6^2 + 2J_2^2 \cos 4w_{RF}t + 4J_2 J_6 \cos 4w_{RF}t \\ &+ 4J_2 J_6 \cos 8w_{RF}t + 2J_6^2 \cos 12w_{RF}t \big] \end{aligned}$$

$$= \Re E_0^2 \cdot \left[\left\{2J_2^2(m) + 4J_2(m)J_6(m)\right\}\cos(4w_{RF}t)\right.$$
$$\left.+4J_2(m)J_6(m)\cos(8w_{RF}t) + 2J_6^2(m)\cos(12w_{RF}t)\right] \quad (10)$$

Equation (10) shows that the photocurrent contains the desired mm-wave signal at $4\omega_{RF}$, which we are interested in, and the harmonic distortion signals with frequency equal to $4n\omega_{RF}$, where $n > 2$, as shown in Fig. 3(b). By utilizing Eq. (10), RFSSR is given by

$$\text{RFSSR} = 20\log\left[\frac{2J_2^2(2.4048)+4J_2(2.4048)J_6(2.4048)}{4J_2(2.4048)J_6(2.4048)}\right] = 36.1\,\text{dB} \quad (11)$$

3. SIMULATION RESULTS AND DISCUSSION

In this section, the performance of the proposed scheme is evaluated through a simulation by using the commercially available simulation software "*OptiSim*^{TM}", which provides numerical modules that enable users to simulate optical components that are commonly used in the optical communication systems. First, the quality of the generated quadrupling-frequency optical mm-wave signal for a B-T-B case is investigated in Section 3.1. The influence of the non-ideal RF-driven voltage and the phase difference between RF-driven signals applied to the two MZMs on OSSR and RFSSR for B-T-B case are then discussed and analyzed in Section 3.2. Finally, the transmission performance of the generated quadrupling-frequency optical mm-wave signal over fiber is investigated in Section 3.3.

3.1. Frequency Quadrupling mm-wave Signal Generation for B-T-B

The simulation system for a B-T-B case is set up as shown in Fig. 1. The LD is assumed to emit the lightwave with a central wavelength of 1552.52 nm, line width of 10 MHz, and power of 0 dBm. The two dual-arm MZMs of the proposed modulator are combined by two optical couplers. The power splitting ratio of the couplers is 0.5. MZM-a and MZM-b are driven by the same RF local oscillator of 15 GHz, with a phase difference of 180° introduced by an electrical phase shifter between the RF-driven signals. The RF-driven signals are applied to the four arms of the two MZMs with different phase shifts introduced by electrical phase shifters, and the four arms are biased by different DC voltages, as depicted in Fig. 1. The half-wave voltage of the MZM is $4v$. The insertion loss of the MZM is 5 dB. Following the modulator, an erbium-doped fiber amplifier (EDFA) with gain of 12 dB and noise figure of 5 dB is utilized to compensate for the insertion loss of the

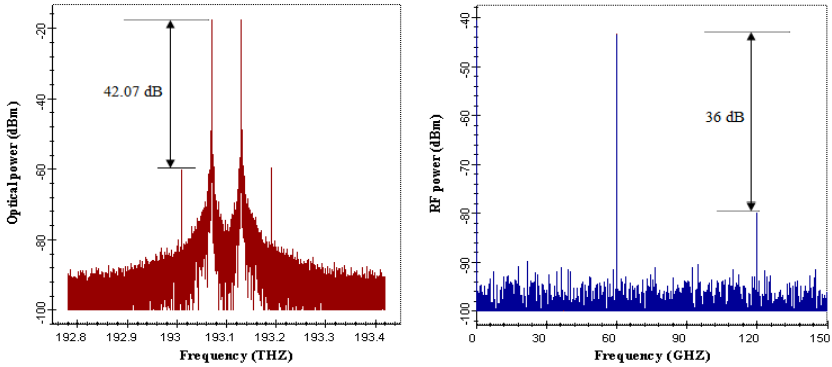

Figure 5. The simulated 60 GHz mm-wave signal generation with 15 GHz RF driven signal for B-T-B, when the extinction ratio is infinite. (a) Optical spectrum. (b) RF spectrum.

modulator. For the PD, the responsivity is $\Re = 0.7\,\mathrm{A/W}$, dark current is 2 nA, and thermal noise is $1 \times 10^{-11}\,\mathrm{A/Hz^{0.5}}$.

Figure 5 shows the simulated results of the optical and RF spectra via the proposed approach when the extinction ratio of the MZM is 100 dB. An extinction ratio of 100 dB can approximately be regarded as infinite. The optical carrier and other undesired sidebands, except for the undesired sixth-order sideband, are completely suppressed. The power of the second-order sideband is −16 dBm, which is significantly higher than that of the sixth-order sideband, and its OSSR is 42.07 dB, as shown in Fig. 5(a). The desired frequency quadrupling 60 GHz mm-wave signal and spurious 120 GHz mm-wave signal are generated simultaneously because of the existence of the undesired sixth-order sideband. Nonetheless, the power of the 60 GHz mm-wave signal is higher than that of the 120 GHz mm-wave signal, and its RFSSR is 36 dB, as shown in Fig. 5(b). Figs. 5(a) and (b) show that the simulation results for the MZM with an infinite extinction ratio are consistent with the theoretical analysis in Section 2 (Eqs. (8) and (11)).

Figure 6 shows the simulated optical and RF spectra for the MZM with an extinction ratio of 25 dB. The power of the second-order optical sideband is maximal, and the OSSR exceeds 39 dB. The power of the 60 GHz mm-wave signal is evidently higher than that of other spurious RF components, and its RFSSR is higher than 35 dB, as shown in Fig. 6(b).

Figure 6 shows that the high-quality quadrupling frequency optical mm-wave signal can be generated without an optical filter for the MZM with an imperfect extinction ratio.

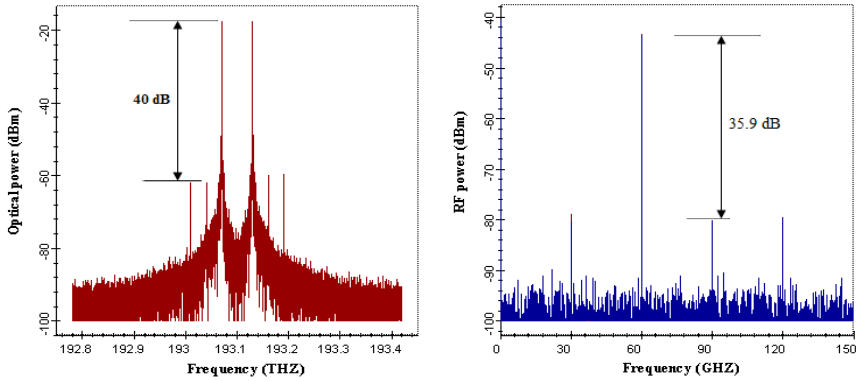

Figure 6. The simulated 60 GHz mm-wave signal generation with 15 GHz RF driven signal for B-T-B, when the extinction ratio is 25 dB. (a) Optical spectrum. (b) RF spectrum.

3.2. Effect of Nonideal RF-driven Voltage and Phase Difference on OSSR and RFSSR for B-T-B

The above theoretical analysis and numerical simulation are based on the assumption that system parameters such as RF driving voltage and phase difference are ideal. Initially, the OSSR can be infinite, but in real systems, non-ideal factors contribute to a finite value: (1) the phase shift may deviate from 180° between the two RF-driven signals applied to MZMs; and (2) the RF-driven voltage may deviate from its desired value. These conditions will result in the degradation of the generated optical mm-wave signal. Therefore, investigating the influence of these non-ideal factors is important. Properly adjusting the related parameters for high-quality mm-wave signal generation is useful. Except for RF-driven voltage and the phase difference between RF-driven signals applied to MZM-a and MZM-b, other parameters are identical to those given in Section 3.1.

Figure 7 shows the effect of phase shift deviation on OSSR. The highest OSSR can be obtained for a phase difference near the ideal value. The value then degrades slowly with the increment of deviation value. An OSSR higher than 22 dB can be obtained if the deviation is within 10°. Compared with OSSR, RFSSR is not influenced by a phase shift deviation with a value of approximately 35.8 dB. This is because the phase shift deviation does not affect the optical carrier suppression ratio. Therefore, the mm-wave at 60 GHz is mainly due to the beating of optical harmonics at $\pm 2w_{RF}$ so that constructive and destructive

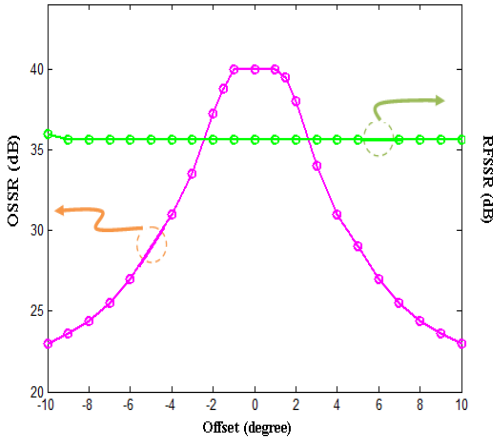

Figure 7. OSSR and RFSSR versus phase shift deviation at an extinction ratio of 25 dB.

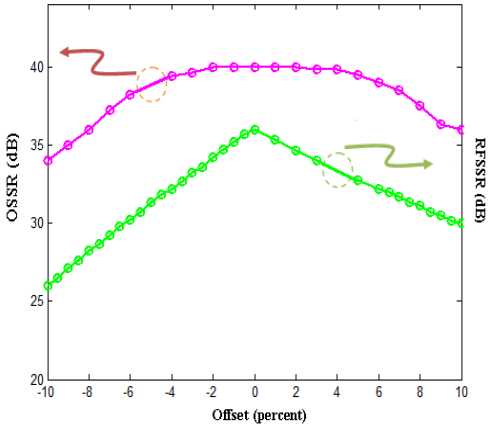

Figure 8. OSSR and RFSSR versus RF driving voltage deviation at an extinction ratio of 25 dB.

interaction hardly occurs so the RFSSR values are not influenced.

The impact of the non-ideal drive voltage of RF-driven signal on OSSR and RFSSR is shown in Fig. 8. OSSR higher than 30 dB and RFSSR higher than 25 dB can be obtained if the deviation is less than 10%. In comparison, RFSSR is more susceptible to nonideal RF driven voltage. This is because the RF driving voltage deviation decreases the

optical carrier suppression ratio. Therefore, the mm-wave at 60 GHz is due to the beating of optical harmonics at $\pm 2w_{RF}$ and beating of sixth-order optical harmonics with the optical carrier so that constructive and destructive interaction will occurs, and the desired mm-wave will suffer from the power fading induced by fiber dispersion.

The quadrupling mm-wave generation scheme is almost unaffected by the deviation of RF-driven voltage, and the non-ideal phase difference has a minimal influence on system performance. The OSSR and RFSSR can respectively be higher than 39 and 35 dB when the extinction ratio is 25 dB. The results are better than those in available reports.

3.3. Transmission Performance of the Generated Quadrupling-frequency Optical mm-wave Signal over Fiber

To further investigate the quality of the generated quadrupling frequency optical mm-wave signal over fiber, we set up an RoF system through simulation, as shown in Fig. 9. Identical parameters are utilized for the identical components in Fig. 1. The simulating spectra at different locations are shown in Fig. 10. After the proposed quadrupling frequency mm-wave generation scheme, two

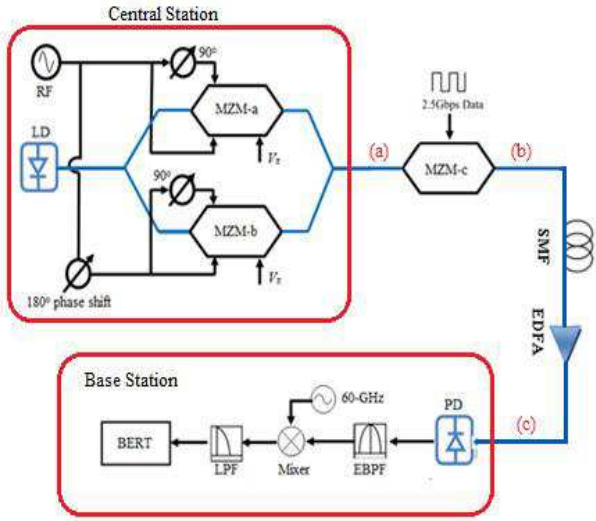

Figure 9. Block diagram of the RoF link based on the proposed quadrupling-frequency optical mm-wave generation approach. (SMF: single-mode fiber; BPF, bandpass filter; LPF, lowpass filter; BERT: bit error rate tester).

optical sidebands of second-order optical harmonics related to the optical carrier are generated and maximized and the frequency spacing between the two sidebands is 60 GHz, as shown in Fig. 10(a). The two second-order sidebands are then intensity modulated with a 2.5 Gbps baseband signal by another MZM (MZM-c) with an extinction of 30 dB, as shown in Fig. 10(b). A single-mode fiber (SMF) with a dispersion of $D = 16.7\,\text{ps/(nm km)}$ and attenuation of $\alpha = 0.23\,\text{dB/km}$ is used in the system, and an erbium-doped fiber amplifier (EDFA) is employed to compensate for both the insertion loss of MZM and fiber loss. At the base station, a PD detects the quadrupling-frequency optical mm-wave, and an electrical first-order Gaussian bandpass filter centered

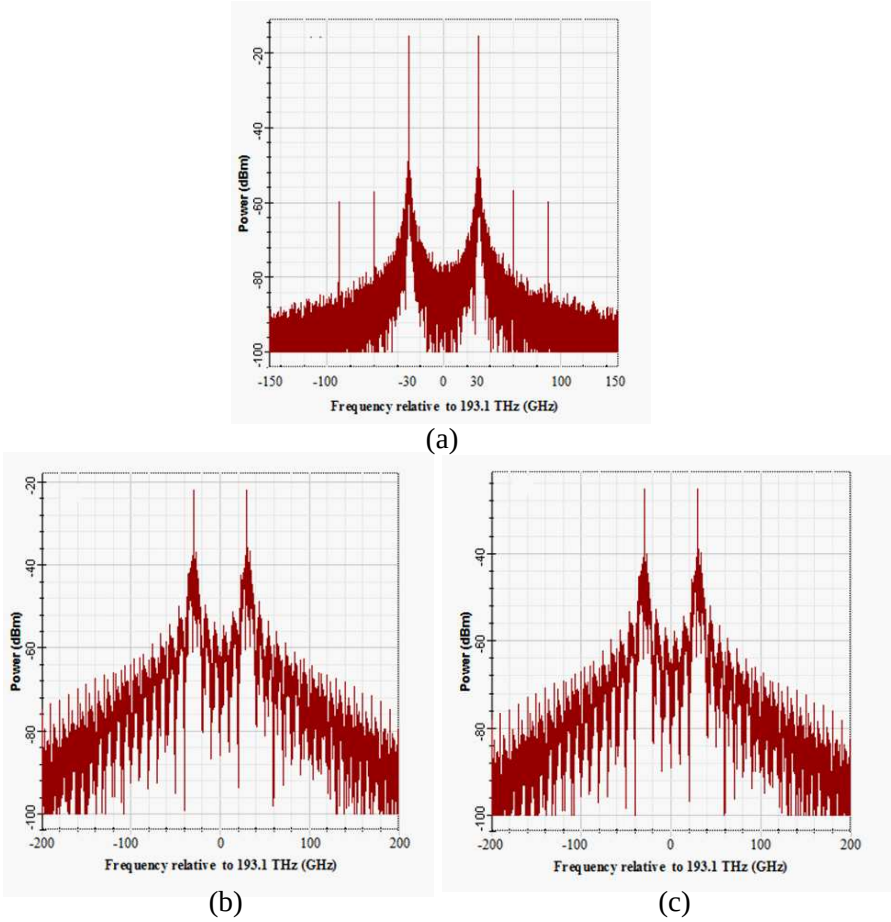

Figure 10. Simulating spectra at different locations corresponding to (a), (b), and (c) located in Figure 9.

at 60 GHz filters out the RF harmonics. To demodulate the baseband signal from the generated 60 GHz mm-wave signal, a 60 GHz RF local oscillator, a mixer, and an electrical first-order Gaussian lowpass filter are utilized. The performance of the system was characterized by referring to the Q-factor and eye pattern.

Figure 11 shows down-converted 2.5 Gbps eye patterns of the 60 GHz mm-wave generated obtained by using the proposed approach

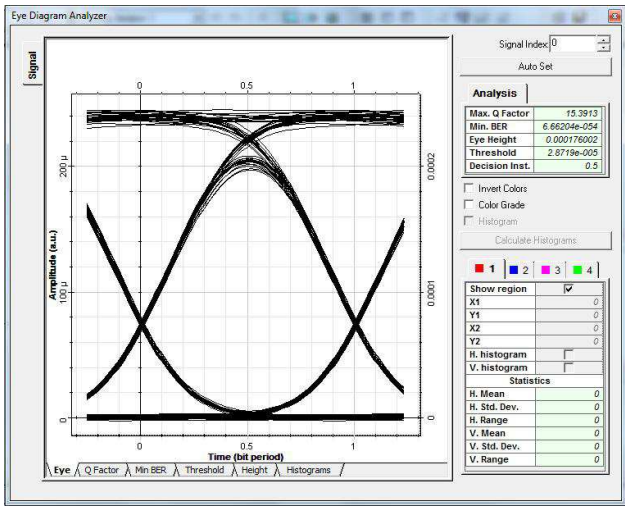

(a)

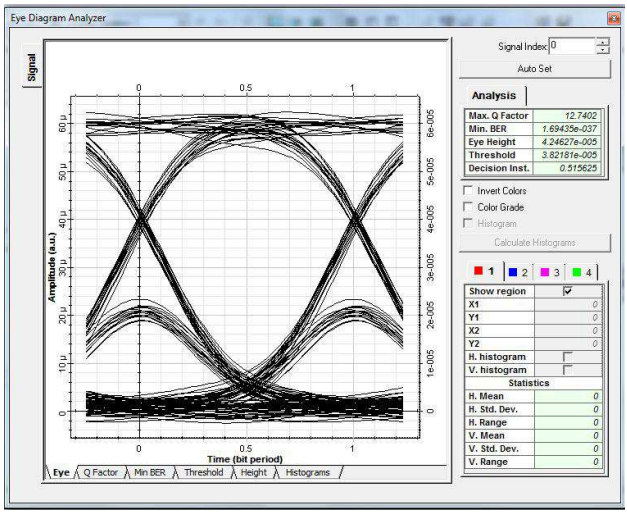

(b)

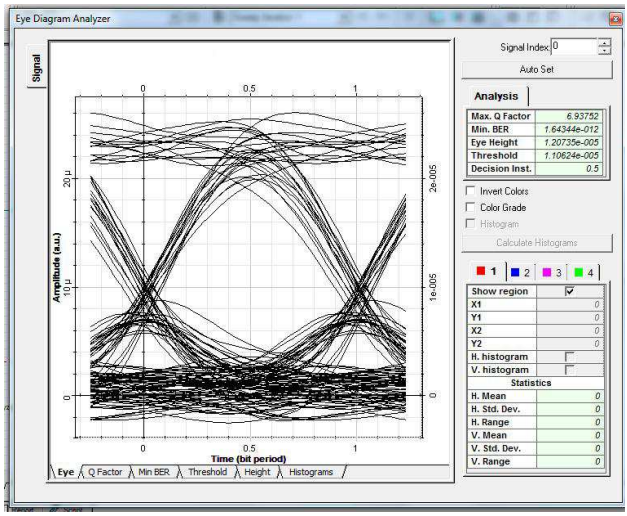

(c)

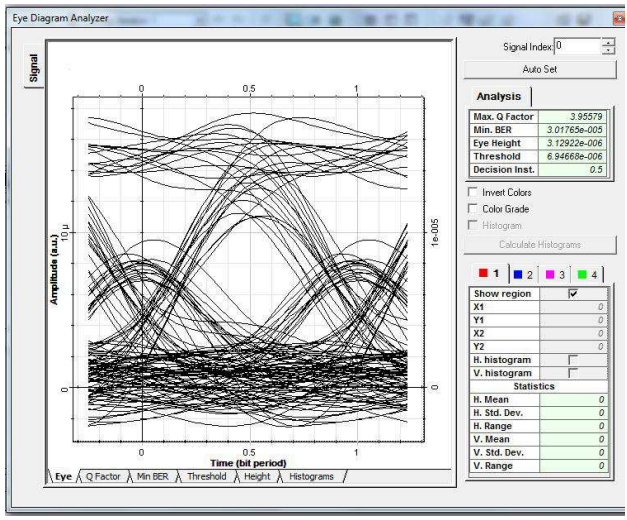

(d)

Figure 11. Simulated eye diagrams of the baseband signals using the proposed OCS quadrupling-frequency at the transmission distance of (a) 20, (b) 40, (c) 60, and (d) 70 km.

after different transmission distances. When the transmission distance is 60 km, the Q-factor is approximately 7 without optical filter, as shown in Fig. 11(c). This is because of the high OSSR of the proposed

scheme. After transmission over 60 km, the Q-factor degraded and reached a value of approximately 4 when the transmission length is 70 km, as shown in Fig. 11(d). The physical cause is the effect of walk-off that induces fiber dispersion [37]. Fig. 11 shows that the outline of the eye patterns changes slightly after different transmission distances. Thus, the generated mm-wave signal is satisfactory.

4. CONCLUSION

We have proposed a new approach for the generation of the OCS quadrupling-frequency optical mm-wave by using two dual-electrode MZMs and have investigated its transmission performance along a single-mode fiber. By using this approach, the desired second-order optical sidebands are maximized, whereas the other optical sidebands are greatly suppressed, so that high frequency up-conversion efficiency is achieved with less nonlinear distortion impact. The simulation results show that a 60 GHz millimeter-wave can be generated from a 15 GHz RF oscillator with an OSSR as high as 40 dB and an RFSSR exceeding 35 dB without any optical or electrical filter when the extinction ratio of the MZM is 25 dB. The influence of non-ideal RF driving voltage and phase difference on OSSR and RFSSR is investigated through a simulation. Results show that although the parameters deviate from the ideal values to a certain degree, the performance remains good, and our scheme is practical for wave-division-multiplexing RoF systems.

REFERENCES

1. Ogawa, H. and D. Polifko, "Fiber optic millimeter-wave subcarrier transmission links for personal radio communication systems," *IEEE MTT-S International Microwave Symposium Digest*, 555–558, 1992.
2. Anang, K. A., P. B. Rapajic, L. Bello, and R. Wu, "Sensitivity of cellular wireless network performance to system & propagation parameters at carrier frequencies greater than GHz," *Progress In Electromagnetics Research B*, Vol. 40, 31–54, 2012.
3. Choudhury, P. K. and W. K. Soon, "On the tapered optical fibers with radially anisotropic liquid crystal clad," *Progress In Electromagnetics Research*, Vol. 115, 461–475, 2011.
4. Huang, T. Y. and T. J. Yen, "A high-ratio bandwidth square-wave-like bandpass filter by two-handed metamaterials and its application in 60 GHz wireless communication," *Progress In Electromagnetics Research Letters*, Vol. 21, 19–29, 2011.

5. Choudhury, P. K., "Transmission through twisted clad liquid crystal optical fibers," *Progress In Electromagnetics Research*, Vol. 131, 169–184, 2012.
6. Sarrazin, T., H. Vettikalladi, O. Lafond, M. Himdi, and N. Rolland, "Low cost 60 GHz new thin Pyralux membrane antennas fed by substrate integrated waveguide," *Progress In Electromagnetics Research B*, Vol. 42, 207–224, 2012.
7. Navarro-Cia, M., V. Torres Landivar, M. Beruete, and M. Sorolla Ayza, "A slow light fishnet-like absorber in the millimeter-wave range," *Progress In Electromagnetic Research*, Vol. 118, 287–301, 2011.
8. Deruyck, M., W. Vereecken, W. Joseph, B. Lannoo, M. Pickavet, and L. Martens, "Reducing the power consumption in wireless access networks: Overview and recommendations," *Progress In Electromagnetics Research*, Vol. 132, 255–274, 2012.
9. Harun, A., D. L. Ndzi, M. F. Ramli, A. Y. M. Shakaff, M. N. Ahmad, L. M. Kamarudin, A. Zakaria, and Y. Yang, "Signal propagation in aquaculture environment for wireless sensor network applications," *Progress In Electromagnetics Research*, Vol. 131, 477–494, 2012.
10. Alejos, A. V., M. Dawood, and L. Medina, "Experimental dynamical evolution of the Brillouin precursor for broadband wireless communication through vegetation," *Progress In Electromagnetics Research*, Vol. 111, 291–309, 2011.
11. Ndzi, D. L., M. A. M. Arif, A. Y. M. Shakaff, M. N. Ahmad, A. Harun, L. M. Kamarudin, A. Zakaria, M. F. Ramli, and M. S. Razalli, "Signal propagation analysis for low data rate wireless sensor network applications in sport grounds and on roads," *Progress In Electromagnetics Research*, Vol. 125, 1–19, 2012.
12. Lin, C. T., et al., "Optical millimeter-wave signal generation using frequency quadrupling technique and no optical filtering," *IEEE Photonics Technology Letters*, Vol. 20, 1027–1029, 2008.
13. Kotb, H. E., M. Y. Shalaby, and M. H. Ahmed, "Generation of nanosecond optical pulses with controlled repetition rate using incavity intensity modulated brillouin erbium fiber laser," *Progress In Electromagnetics Research*, Vol. 113, 313–331, 2011.
14. Calo, G., D. Alexandropoulos, and V. Petruzzelli, "Active WDM filter on dilute nitride quantum well photonic band gap waveguide," *Progress In Electromagnetics Research Letters*, Vol. 35, 37–49, 2012.
15. Jia, Z., et al., "Key enabling technologies for optical wireless

networks: Optical millimeter-wave generation, wavelength reuse, and architecture," *Journal of Lightwave Technology*, Vol. 25, 3452–3471, 2007.

16. Kumar, A., B. Suthar, V. Kumar, K. S. Singh, and A. Bhargava, "Tunable wavelength demultiplexer for DWDM application using 1-D photonic crystal," *Progress In Electromagnetics Research Letters*, Vol. 33, 27–35, 2012.
17. Kapilevich, B. and B. Litvak, "Noise versus coherency in mm-wave and microwave scattering from nonhomogeneous materials," *Progress In Electromagnetics Research B*, Vol. 28, 35–54, 2011.
18. Yu, J., et al., "Optical millimeter-wave generation or up-conversion using external modulators," *IEEE Photonics Technology Letters*, Vol. 18, 265–267, 2006.
19. Ma, J., et al., "Optical mm-wave generation by using external modulator based on optical carrier suppression," *Optics Communications*, Vol. 268, 51–57, 2006.
20. Zavargo-Peche, L., A. Ortega-Monux, J. G. Wanguemert-Perez, and I. Molina-Fernandez, "Fourier based combined techniques to design novel sub-wavelength optical integrated devices," *Progress In Electromagnetics Research*, Vol. 123, 447–465, 2012.
21. Qi, G., et al., "Generation and distribution of a wide-band continuously tunable millimeter-wave signal with an optical external modulation technique," *IEEE Transactions on Microwave Theory and Techniques*, Vol. 53, 3090–3097, 2005.
22. Liu, J., L. Zhang, S.-H. Fan, C. Guo, S. He, and G.-K. Chang, "A novel architecture for peer-to-peer interconnect in millimeter-wave radio-over-fiber access networks," *Progress In Electromagnetics Research*, Vol. 126, 139–148, 2012.
23. Qi, G., et al., "Optical generation and distribution of continuously tunable millimeter-wave signals using an optical phase modulator," *Journal of Lightwave Technology*, Vol. 23, 2687–2695, 2005.
24. Wang, H., B. Yan, Z. Wang, and R.-M. Xu, "A broadband microwave gain equalizer," *Progress In Electromagnetics Research Letters*, Vol. 33, 63–72, 2012.
25. Ou, H., et al., "Microwave-photonic frequency doubling utilising phase modulator and fibre Bragg grating," *Electronics Letters*, Vol. 44, 131–133, 2008.
26. Chen, L., et al., "A radio-over-fiber system with a novel scheme for millimeter-wave generation and wavelength reuse for up-link connection," *IEEE Photonics Technology Letters*, Vol. 18, 2056–

2058, 2006.

27. Zakeri, B. G., M. R. Zahabi, and S. Alighale, "Sidelobes level improvement by using a new scheme used in microwave pulse compression radars," *Progress In Electromagnetics Research Letters*, Vol. 30, 81–90, 2012.
28. He, J., et al., "Full-duplex radio-over-fiber system with photonics frequency quadruples for optical millimeter-wave generation," *Optical Fiber Technology*, Vol. 15, 290–295, 2009.
29. Yu, J., et al., "Centralized lightwave radio-over-fiber system with high-frequency optical millimeter-wave generation by low-frequency and low-bandwidth optical and electrical sources," *IEEE International Topical Meeting on Microwave Photonics*, 127–129, 2007.
30. Deng, L., et al., "42.13 Gbit/s 16QAM-OFDM photonics-wireless transmission in 75–110 GHz band," *Progress In Electromagnetics Research*, Vol. 126, 449–461, 2012.
31. Zhang, J., et al., "A photonic microwave frequency quadrupler using two cascaded intensity modulators with repetitious optical carrier suppression," *IEEE Photonics Technology Letters*, Vol. 19, 1057–1059, 2007.
32. Lu, H. H., et al., "Radio-over-fiber transport systems based on dfb ld with main and −1 side modes injection-locked technique," *Progress In Electromagnetics Research Letters*, Vol. 7, 25–33, 2009.
33. Chen, et al., "A novel optical mm-wave generation scheme based on three parallel Mach-Zehnder modulators," *Optics Communications*, Vol. 284, 1159–1169, 2011.
34. Zhao, Y., et al., "Simplified optical millimeter-wave generation configuration by frequency quadrupling using two cascaded Mach-Zehnder modulators," *Optics Letters*, Vol. 34, 3250–3252, 2009.
35. Liu, X., et al., "Frequency quadrupling using an integrated Mach-Zehnder modulator with four arms," *Optics Communications*, Vol. 284, 4052–4058, 2011.
36. Błahut, M. and A. Opilski, "Multimode interference structures — New way of passive elements technology for photonics," *Opto-electronics Review*, Vol. 9, 293–300, 2001.
37. Ma, J., et al., "Fiber dispersion influence on transmission of the optical millimeter-waves generated using LN-MZM intensity modulation," *Journal of Lightwave Technology*, Vol. 25, 3244–3256, 2007.